# AMERICAN METEOROLOGICAL SOCIETY
**AMS Journals Online**

## Full Text View

# Decadal Variability of North Pacific Central Mode Water[*]

**Carol Ladd**

*Pacific Marine Environmental Laboratory, NOAA, Seattle, Washington*

**LuAnne Thompson**

*School of Oceanography, University of Washington, Seattle, Washington*

### ABSTRACT

An isopycnal model forced with wind stress and heat fluxes from 1965 through 1993 was used to examine the effects of variable atmospheric forcing on the ventilation of the North Pacific. During this time period, a climatic regime shift occurred that had significant impacts on heat fluxes, sea surface temperature (SST), and wind stress patterns. The climate shift, occurring in the winter of 1976/77, affected the formation rates and locations, and properties of the Central Mode Water (CMW) formed in the model. Three model runs were compared: one with variable buoyancy forcing and climatological wind forcing, one with variable wind forcing and climatological buoyancy forcing, and one with variability in both the buoyancy and the wind forcing. The comparison indicates that buoyancy forcing is of primary importance in the variability of mode water formation and properties surrounding the climate shift. One measure of the climate shift is the Pacific decadal oscillation (PDO), an index of SST variability in the North Pacific, which changed sign in 1976/77. A positive state for the PDO is associated with deeper model mixed layers, formation of denser varieties of CMW, and an anticyclonic circulation anomaly in the CMW density range.

## 1. Introduction

There is significant decadal variability in the midlatitude North Pacific that manifests itself in sea surface temperature (e.g., Namias 1969; Namias et al. 1988; Nitta and Yamada 1989; Trenberth 1990; Graham 1994; Trenberth and Hurrell 1994). This variability is correlated with winter weather variability over North

America ([Latif and Barnett 1994](#), [1996](#)), surface air temperatures and snow extent over Eurasia ([Watanabe and Nitta 1999](#)), and salmon production in the North Pacific ([Hare and Francis 1995](#); [Mantua et al. 1997](#)). The SST and associated changes in other climate characteristics in the North Pacific have been described as "regime shifts" in which the mean conditions change abruptly ([Ebbesmeyer et al. 1991](#); [Latif and Barnett 1994](#); [Mantua et al. 1997](#); [Zhang et al. 1997](#)). The Pacific decadal oscillation (PDO) the leading mode of sea surface temperature (SST) variability in the North Pacific, has timescales of 20–30 years. Regime shifts, evident in the PDO index ([Fig. 1](#) ⊙▬), have been identified in 1925, 1947, and 1977 ([Mantua et al. 1997](#)).

Decadal variability is seen in the ocean interior as well as at the surface. [Deser et al. (1996)](#) document a series of cold pulses beginning in the autumn of 1976 and continuing until 1988. These pulses originate at the surface and descend with time to at least 400-m depth. Using both data and model results, [Miller et al. (1998)](#) calculate extended empirical orthogonal functions (EEOFs) for 400-m temperature anomalies. They find two dominant modes of variability that both exhibit decadal timescales. Both data and model results exhibit the first EEOF, which is dominated by a stationary pattern between 30° and 45°N that increases in amplitude toward the west. The time variation of this mode shows that in the early 1970s, the temperature at 400 m was anomalously warm in the northwestern Pacific and reversed sign around 1979 to anomalously cool temperatures. They attribute this mode to a Sverdrup response to decadal changes in basin-scale wind stress curl. In fact, their model subpolar and subtropical gyres strengthen by roughly 10% from the 1970s to the 1980s. In support of these conclusions, [Deser et al. (1999)](#) find that the decadal changes in Sverdrup transport inferred from the wind stress curl field are consistent with the observed geostrophic flow derived from XBT data in both spatial pattern and magnitude. The second EEOF (in the data only) calculated by [Miller et al. (1998)](#) is concentrated in the central and eastern North Pacific. [Miller et al. (1998)](#) associate this mode with anomalous subduction, likely related to the formation of Central Mode Water (discussed below). Their model failed to reproduce this second mode. This failure may be owing to a lack of density resolution in the model resulting in a failure to reproduce mode water formation in the central Pacific.

Mode water formation occurs in localized regions where subduction rates are large. These regions are important in transmitting the effects of atmospheric forcing to the sub-surface ocean. In the North Pacific, three kinds of mode waters have been identified: North Pacific Subtropical Mode Water (STMW) in the western North Pacific ([Masuzawa 1969](#)), Central Mode Water (CMW) in the central North Pacific ([Nakamura 1996](#); [Suga et al. 1997](#)), and Eastern Subtropical Mode Water (ESMW) in the eastern North Pacific ([Hautala and Roemmich 1998](#); [Ladd and Thompson 2000](#)).

Here we focus on the CMW as it has the largest volume of all of the North Pacific mode waters, and is located in the region in the water column where models and observations have shown significant variability ([Deser et al. 1999](#); [Miller et al. 1998](#)). The CMW pycnostad is identified by low potential vorticity (PV) on the $\sigma_\theta = 26.2$ kg m$^{-3}$ isopycnal surface in the central subtropical gyre ([Talley 1988](#)). This isopycnal is shallower than 400 m in the region of the PV minimum and therefore is included in the analyses of [Deser et al. (1996](#), [1999)](#) and [Miller et al. (1998)](#) discussed above. By analyzing $T$–$S$ diagrams limited to parcels of water with PV less than $1.5 \times 10^{-10}$ m$^{-1}$ s$^{-1}$, [Nakamura (1996)](#) estimated a characteristic $\sigma_\theta$ range of 26.0–26.5 kg m$^{-3}$ for CMW. The formation region for CMW is located north of the Kuroshio Extension and east of ~ 170°E ([Nakamura 1996](#)). This is east of the STMW formation region (south of the Kuroshio Extension between 140° and 170°E). We have suggested that preconditioning supplied by the STMW formation allows the CMW to form ([Ladd and Thompson 2000](#)). Heat losses in the CMW formation region are of order 200 W m$^{-2}$ weaker than in the STMW formation region but mixed layer depths are as deep or deeper than in the STMW formation region (MLD > 200 m in STMW formation region; MLD > 240 m in CMW formation region; [Ladd and Thompson 2000](#)).

Because CMW is formed in the central North Pacific where the observed subducted temperature anomalies originate ([Deser et al. 1996](#); [Pierce et al. 2000](#); [Schneider et al. 1999](#); [Zhang and Liu 1999](#)), the CMW may be the most important of the North Pacific mode waters in the link between decadal climate variability and subduction. The renewal time for the CMW is about 15 yr, and anomalies may be sequestered from further contact with the atmosphere over this time period. Then they may reemerge to influence SST through reentrainment into the mixed layer. Thus the influence of climate variability on mode water formation rates, properties, and location may be important in the midlatitude ocean and atmosphere system.

Using SST, wind stress, and heat flux data, [Yasuda and Hanawa (1997)](#) document changes in North Pacific subtropical and central mode water properties following the 1976/77 climate shift. They find that the CMW and the northeastern part of the STMW became colder, while the southwestern part of the STMW became warmer in the decade after the climate shift. However, due to the effects of mesoscale eddies, they were unable to show that the temperature differences are statistically significant.

In this model study, we concentrate on the influence of decadal variability in atmospheric forcing on the formation rates and properties of the CMW and diagnose how the interior pycnocline waters carry climate regime shift signals. The model permits evaluation of the mechanisms important in linking the CMW to changes in surface conditions. We investigate whether the model exhibits results similar (in density rather than temperature) to those of [Yasuda and Hanawa (1997)](#),

lending support to their analysis. In addition, by using a model, we can analyze variability in formation rates and gyre circulation that are difficult to investigate using observational data.

The remainder of this paper is organized as follows: Section 2 includes a description of the model. Section 3 describes the 1976/77 regime shift. Section 4 describes the variability of the CMW, focusing on changes surrounding 1976/77. In addition, a short discussion of the variability of STMW and ESMW is included. Section 5 explores the relationship between CMW variability and the PDO climate index. And section 6 provides discussion and conclusions.

## 2. Model description

The model used for this study is the Hallberg Isopycnal Model (Hallberg 1995; Ladd and Thompson 2001; Thompson et al. 2002). It is configured with 16 layers in the vertical including a Kraus and Turner (1967) bulk mixed layer, a variable density buffer layer to handle mixed layer detrainment, and 14 isopycnal layers. [See Ladd and Thompson (2001) for details regarding the buffer layer and model initialization.]

The layer densities were chosen in an attempt to distinguish the various mode water masses (Subtropical, Central, and Eastern Subtropical Mode Waters) observed in the North Pacific (Table 1 ⬤▬). The model domain (20°S to 60°N, 126°E to 76°W) covers the entire North Pacific with realistic topography and coastline and a horizontal resolution of 2°. Layer thicknesses are continually relaxed to winter climatological values in the Sea of Okhotsk. We found that this helped correct for the inadequacy of North Pacific Intermediate Water (NPIW) formation in the model and resulted in a more realistic thermocline structure. However, analysis of a model run without the relaxation in the Sea of Okhotsk did not substantially change our results.

After an initial 30-yr spinup using climatological forcing, the model is forced at the surface with daily linear interpolations of monthly heat fluxes (converted to density fluxes) and surface winds from January 1965 to December 1993. In addition, the surface density fluxes include climatological freshwater flux forcing. All forcing fields are taken from the *Atlas of Surface Marine Data 1994* (da Silva et al. 1994, hereafter ASMD). To keep surface density values from drifting too far from reality, we relax the mixed layer density to daily interpolations of observed monthly surface density with a relaxation timescale of 35 days. The observed monthly surface density is calculated using climatological salinity (Levitus et al. 1994) and sea surface temperature anomalies from the ASMD added to climatological sea surface temperature from Levitus and Boyer (1994). The density flux per mixed layer volume at the surface is

$$ f = -\frac{\alpha Q}{C_p} + \frac{h}{\lambda}(\rho_{obs} - \rho_{model}) + \beta S(E - P), \quad (1) $$

where $Q$ (W m$^{-2}$) is the monthly varying net heat flux from the atmosphere to the ocean (the sum of radiative, latent, and sensible fluxes) from the ASMD, $\alpha$ (K$^{-1}$) is the thermal expansion coefficient (monthly and latitudinally varying), $C_p$ (J kg$^{-1}$ K$^{-1}$) is the specific heat, $h$ is an average mixed layer depth (taken to be 100 m), $\lambda$ is a relaxation timescale (35 days), $\rho_{obs}$ is surface density calculated from interannually varying temperature and climatological salinity, $\rho_{model}$ is the surface density calculated from the model, $\beta$ is the haline contraction coefficient (0.775 kg m$^{-3}$ psu$^{-1}$), $S$ is surface salinity (35 psu), and $E{-}P$ (m s$^{-1}$) is climatological evaporation rate minus precipitation rate from the ASMD.

In addition to the fully variable model run described above, two additional runs were executed to distinguish between the effects of wind forcing variability and buoyancy forcing variability. The variable wind-forcing run used the same wind forcing as the fully variable run described above but the buoyancy forcing consisted of a mean annual cycle and surface density was relaxed to monthly climatological values. The variable buoyancy-forcing run used the same monthly variable buoyancy forcing and surface density relaxation described for the fully variable run but was forced with monthly climatological winds.

In the region of interest in this study, the Kuroshio Extension and the CMW formation and distribution region, the total surface density flux is primarily determined by the surface heat flux. In localized regions, particularly in the eastern Tropics, the relaxation term in (1) has a magnitude comparable to the surface heat flux term. This helps to correct for limited density resolution at lighter densities there. Density flux due to $E{-}P$ is also small compared to the heat flux term in the region of interest.

## 3. The 1976/77 climate shift

The 1976/77 regime shift was first described as a strengthening of the Aleutian low, a drop in SST in the central Pacific,

and a rise in SST in the eastern Pacific (Namias 1978; Nitta and Yamada 1989; Trenberth 1990). By calculating a mixed layer heat budget, Miller et al. (1994) find that anomalously strong cooling by horizontal advection combined with anomalous surface cooling during the year prior to the shift instigated the change in SST. In addition, they find that entrainment from below contributed to the maintenance of the cool (warm) SST after (before) the shift. Yasuda and Hanawa (1997) compare heat fluxes and Ekman heat divergences between the decade before and the decade after the climate shift. They conclude that the temperature decrease (density increase) in the central North Pacific is due to a combination of a larger amount of heat released from the ocean and an increased southward Ekman transport of cold water due to the intensification of the westerlies with the Ekman transport dominating. The mixed layer density budget from our model (not shown) is consistent with the conclusions of Miller et al. (1994) and Yasuda and Hanawa (1997).

The difference in winter [December–February (DJF)] heat fluxes between the five years following the climate shift (average of 1977–81 winters) and the five years preceding (1972–76) (Fig. 2a ⊙) shows that heat loss was more than 20 W m$^{-2}$ stronger in a band along ~ 35°N after the climate shift. In contrast, the ocean gained heat in the eastern part of both the subtropical and subpolar gyres in 1977–81 relative to 1972–76. The difference in wind stress between the two pentads (Fig. 2b ⊙) illustrates the influence of a stronger Aleutian low (Hanawa et al. 1996; Trenberth and Hurrell 1994) with stronger westerly winds in a broad band from approximately 20° to 35°N. The heat flux and wind stress differences are similar to the patterns associated with the PDO (see Fig. 9 ⊙ and discussion in section 5).

Differences in forcing lead to differences in winter surface density between the pentads. After the 1977 climate shift, surface density in the central North Pacific increases by more than 0.1 kg m$^{-3}$ with a corresponding decrease along the west coast of North America (Fig. 3 ⊙). The surface density shift shown in Fig. 3 ⊙ is very close to that observed. The denser surface waters in the central North Pacific after 1977 imply a southeastward shift in isopycnal outcrop locations. Because an isopycnal surface interacts with the atmosphere only where it outcrops into the mixed layer, a change in outcrop location (without a corresponding change in atmospheric forcing) exposes isopycnal surfaces to different atmospheric forcing in the two decades. This influences the intensity and region of mode water formation and the density at which it forms (discussed in the next section).

## 4. Decadal changes in CMW

First we will describe how the CMW changed between the pre-1976 pentad and the post-1976 pentad. Then we will diagnose the mechanisms involved in those changes. Because mode waters are defined as relatively homogeneous layers of water, they can be identified and traced using minima in PV (McCartney 1982). Following Ladd and Thompson (2001), we define the CMW region as 15°–50°N, 140°E–120°W, encompassing the PV minimum. Next, we define CMW to be any layer 10–12 water (Table 1 ⊙) in this region that has PV less than $1.0 \times 10^{-10}$ m$^{-1}$ s$^{-1}$.

### a. CMW properties

Using this definition for CMW, the mean density of the CMW in the fully variable run is 26.05 kg m$^{-3}$ averaged over 1970–76 and 26.11 kg m$^{-3}$ averaged over 1977–82 (Fig. 4a ⊙). From 1974 until 1986, the CMW exhibits a monotonic trend toward increasing density. A similar pattern results from the buoyancy variability model run. On the other hand, the wind variability run results in much smaller amplitude of variability of CMW density with no discernable shift in the mid-1970s suggesting that variability in buoyancy forcing is primarily responsible for the observed increase in CMW density. The density increase is consistent with cooling of the CMW core temperature from 9°–14°C in 1966–75 to 8°–13°C in 1976–85 found by Yasuda and Hanawa (1997).

The annual maximum CMW volume describes the volume of mode water in the spring after the mixed layer has detrained into the subsurface layers. The annual minimum volume describes the amount of mode water that has escaped mixed layer reentrainment during the period when the mixed layer is the deepest. The minimum volume averages just over 50% of the maximum volume, implying that 50% of the CMW moves far enough from the formation region to escape reentrainment into the mixed layer in the succeeding year. Mean volumes increase by roughly 30% between the decade before 1976 and the decade after (Fig. 5 ⊙), consistent with the observed wider distribution of CMW after 1976 (Yasuda and Hanawa 1997). The buoyancy variability run (but not the wind variability run) also results in increased CMW volume after 1976. In fact, the effects of wind variability appear to counteract the effects of buoyancy variability in the fully variable run. As we discuss in the next two sections, the primary effect of variability in the wind forcing is to change the location of the CMW due to changes in the gyre structure. On the other hand, by influencing mixed layer depth and surface density, variability in the buoyancy forcing tends to change formation rates and locations influencing the volume and density of CMW.

### b. CMW formation

Mode water is formed when low PV (low stratification) water exits the mixed layer and penetrates into a subsurface layer.

The subduction of water from the mixed layer into the permanent pycnocline is accomplished through Ekman pumping and lateral induction (Marshall et al. 1993). The lateral induction term, where water is advected across the sloping mixed layer base, has been found to be most important in the formation of CMW (Huang and Qiu 1994; Nakamura 1996). This is consistent with the study of Inui et al. (1999) who find that the path of the low PV water on each isopycnal starts from the point where the isopycnal outcrop intersects with the mixed layer depth front, the region of high horizontal gradients in winter mixed layer depth. The overlap of deep mixed layer regions with isopycnal layer outcrops is critical in this process. The deep mixed layers provide the low PV water, and the layer outcrop sets the density and provides the pathway into the interior. Once the mode water has been isolated from surface forcing, horizontal advection can move and spread the mode water away from the formation region.

Although the isopycnal outcrop location shifts southeastward after the climate shift, the location of the mixed layer depth front does not change much (Fig. 6 ). This implies that mode water will be formed in much the same region, but at a different density. Most of the mixed layer depth maximum occurs at surface densities between 26 and 26.25 kg m$^{-3}$ (primarily ventilating layer 11) in the later pentad and between 25.75 and 26 kg m$^{-3}$ in the earlier pentad (ventilating layer 10). This results in mode water being formed in denser layers in the model during the latter pentad. In addition, the mixed layer depth maximum is deeper and depths greater than 400 m occur over a broader area after the climate shift. Mode water is formed when the well-mixed water detrains from the mixed layer into the subsurface isopycnal layers and then is advected to a region where it will not be reentrained into the mixed layer in the succeeding year. Thus, a broader region of deeper mixed layer leads to higher formation rates and larger mode water volumes.

The overlap of the surface density outcrops with mixed layer depth for the buoyancy variability run looks almost the same as for the fully variable run. The wind variability run exhibits almost no change between the two pentads (not shown). In an idealized model, Inui et al. (1999) find that intensified cooling results in changes in density of ventilated water while intensified westerly winds result in a shift of ventilation location. Our results suggest that changes in CMW formation surrounding the 1976/77 climate shift are primarily due to changes in buoyancy forcing.

Variation in the formation of CMW can be diagnosed by examining the difference in flux into layers 10, 11, and 12 between the pentad preceding and the pentad following the shift (Fig. 7 ). The flux into a layer, which we will call "layer flux," includes flux to (from) the mixed layer when the mixed layer entrains (detrains) and diapycnal diffusion between layers. Note that, because of the PV restriction in the definition of CMW, fluxes into layers 10, 11, or 12 do not directly translate into formation of mode water. However, differences in layer fluxes between the pentads do show the differences in formation of different density classes.

In all three layers, layer fluxes increase and shift southeastward in the pentad after the climate shift, illustrating that formation of subsurface water in these density classes increased after 1976. Flux into layer 12 increases twice as much as flux into layers 10 and 11, contributing to the increase in density of the CMW after 1976. The increase in formation also translates into an increased volume of CMW (Fig. 5 ). Because the low PV tongue that defines the mode water advects southeastward away from the outcrop, the PV minimum that remains during the winter period of deep mixed layers is southeast of the formation region. Thus, when the layer fluxes shift southeastward, they move toward the PV minimum left over from previous years, directly ventilating the CMW.

## c. CMW core location

The location of the meridional PV minimum can vary by as much as 10° of longitude (Fig. 8 ). This variability in the longitude of the mode water core was also observed in the model run of Xie et al. (2000). Their model, forced with variable wind forcing but climatological buoyancy forcing, shows a westward shift in the mode water core at 36°N in the late 1960s and an eastward shift in the early 1980s. In the wind variability model run, a similar eastward shift (due to changes in the shape of the gyre) in the location of the mode water core from the late 1970s to the late 1980s is observed in layers 10 and 11 (Fig. 8 ). However in the buoyancy variability run, the model results in a westward shift over the same time period due to a westward shift in the formation region. The full model run, including variability in both wind and buoyancy forcing appears to be essentially a linear combination of the two cases, with reduced variability in the longitude of the mode water core.

The longitude of the PV minimum on each isopycnal can vary due to a change in the location of formation or a change in advection (after formation). In addition, when we define a PV minimum over multiple layers (a center of mass of the mode water), the center of mass can shift longitude due to changes in mode water density because denser layers are ventilated farther to the east. Xie et al. (2000) attribute the shift in the location of the PV minimum on select isopycnals primarily to a change in the strength of the zonal advection between the two decades. However, variability in buoyancy forcing (neglected in Xie et al.'s model) has a large influence on the magnitude and location of formation. According to our model runs, the change in advection due to changes in the wind forcing between the two decades acts to shift the CMW to the east in the 1980s. Changes in the magnitude and location of formation due to changes in the buoyancy forcing tend to shift the CMW core to the west during the same time period. In addition, the buoyancy forcing also acts to increase the formation of denser

(layer 12) CMW, which would tend to shift the mode water center of mass location to the east. The combination of these competing influences results in smaller amplitude and higher frequency (interannual instead of decadal) of CMW location variability.

Our results show that, when formation in a particular density class is strong, the longitude of the formation region for that particular density determines the longitude of the PV minimum on that layer. However, when formation is weak (as in layer 12 after 1989), then the PV minimum attributable to mode water formed in previous years determines the PV minimum on the isopycnal. In this case, advection determines the location of the PV minimum. Eastward advection is particularly apparent in layer 12 with the PV minimum moving 20° of longitude over approximately 5 years ($\sim 1$ cm s$^{-1}$), consistent with zonal advection speeds in layer 12. In addition, the center of mass of the PV minimum at 35°N moves eastward in the 1980s compared with the 1970s due to the increased density of the mode water (not shown).

## d. Subtropical mode water

Yasuda and Hanawa (1997) found that the southwestern part of the subtropical mode water warmed after the 1976/77 climate shift. They attributed this warming to increased advection of warm water from lower latitudes due to the subtropical gyre spinup. Our model results show decreasing density of STMW after the climate shift in the fully variable and the variable wind runs but not the variable buoyancy run (Fig. 4b ⊙). The surface density budget shows that the decrease in density in the STMW formation region (at around 35°N near the western boundary) is due primarily to the effects of advection and entrainment (not shown), supporting Yasuda and Hanawa gyre spinup hypothesis.

## e. Eastern subtropical mode water

The modeled density of eastern subtropical mode water also exhibits decadal-scale variations with minimum density in the winter of 1976 and maxima in 1970 and in the early 1980s (Fig. 4c ⊙). This variability appears to be solely due to variability in buoyancy forcing. In the period from 1977 to 1988, the eastern mixed layer depth maximum is broader than the periods before and after. Thus, from 1977 to 1988, denser layers outcropping to the northwest of the usual ESMW formation region are also influenced by the deeper mixed layers allowing the ESMW to be denser. In the periods from 1972 to 1976 and 1989 to 1993, the mixed layer depth maximum associated with ESMW formation is more localized and separated from the band of deep mixed layer depths in the west. This results in ESMW that is more confined to the lighter layers.

## 5. Relationship with PDO

Since the ventilation of the densest CMW layer (12) in our model is intimately linked to the decadal variability of the CMW, with denser varieties of CMW forming during some periods but not during others, relationships between the PDO index (Fig. 1 ⊙) and layer 12 variability were explored in more detail. The SST pattern associated with the positive phase of the PDO consists of cool anomalies in the central North Pacific and warm anomalies along the coast of North America (Fig. 9a ⊙). Regressions show that the PDO has sea level pressure (SLP) and heat flux signatures as well. When the PDO is in a positive phase, SLP tends to be anomalously low over the entire North Pacific north of 30°N (Fig. 9b ⊙). The SLP pattern is consistent with enhanced westerly winds over the central North Pacific (from 30° to about 50°N). Also associated with the positive phase of the PDO is enhanced cooling of the ocean over the Kuroshio Extension region and warming in the Gulf of Alaska (Fig. 9c ⊙).

Regression analysis shows significant correlations between September layer 12 thickness and the previous winter (November–March) PDO time series in the CMW formation region (Fig. 10 ⊙), implying that processes associated with the PDO influence the formation of CMW. The maximum thickness anomaly correlated with the PDO is large, about 65 m, approximately 25% of the average September layer 12 thickness in this region. The maximum correlation coefficient is about 0.7. Note that the thickness anomaly associated with the PDO echoes the layer 12 flux difference between the two pentads surrounding the 1976/77 climate shift (Fig. 7c ⊙) suggesting that the primary PDO influence on layer 12 thickness (and thus CMW density) is through convective fluxes into the layer. Regressions between the PDO and layer 11 thickness exhibit a smaller, less significant pattern (not shown).

Regressions between March mixed layer depth and the PDO show significant correlations in the CMW formation region (Fig. 11 ⊙). The maximum mixed layer depth anomaly correlated with the PDO (correlation coefficient $\sim 0.7$) is about 110 m, approximately 25% of the model mean March mixed layer depth in this region. In addition, formation rates for both layer 11 and layer 12 are correlated with the PDO in a pattern similar to Fig. 7 ⊙, the difference between the two pentads surrounding 1976/77.

The PDO time series is significantly correlated with the layer-12 streamfunction in a pattern centered on the CMW formation region (Fig. 12 ⊙). The maximum correlated streamfunction anomaly is about 0.4 Sv with a correlation

coefficient of $\sim 0.6$. In the buoyancy variability model run, a similar streamfunction correlation pattern is found (not shown). This is consistent with heat flux variability associated with the PDO driving the formation of low PV water in layer 12, which influences the regional circulation. In the wind variability run, no significant correlations were found between the PDO and the layer-12 streamfunction. The barotropic streamfunction on the other hand, is primarily driven by the wind forcing variability. It is weakly correlated with the PDO at a magnitude of $\sim 1.0$ Sv (Sv $\equiv 10^6$ m$^3$ s$^{-1}$), too small to account for the 10% increase in gyre circulation attributed to the 1976/77 climate shift.

In summary, positive PDO (cool SST in central North Pacific; warm SST along coast of North America) is associated with deeper mixed layers, denser CMW (thicker layer 12), and an anticyclonic circulation anomaly, all centered on the CMW formation region. Because winter cooling is the primary mechanism for deepening the mixed layer in this region (Ladd and Thompson 2000), this suggests that surface buoyancy forcing is the mechanism through which PDO-related forcing influences CMW formation.

## 6. Discussion

An isopycnal model forced with wind stress and heat fluxes from 1965 through 1993 was used to examine the effects of variable atmospheric forcing on the ventilation of the North Pacific. During this time period, a climatic regime shift occurred that had significant impacts on heat fluxes, SST, and wind stress patterns. After the winter of 1976/77, the central North Pacific SST became colder and the band of westerly winds between 20° and 45°N became stronger. The climate shift had significant effects on the formation rates and locations, and properties of the CMW formed in the model.

The model forms a PV minimum in the central North Pacific in layers 10, 11, and 12 ($25.875 < \sigma_\theta < 26.375$) that corresponds to the CMW. This density range is wider than that observed for the CMW because of the coarse vertical resolution in the model. Because of changes in the surface density fluxes, the density outcrops shift southeastward after the winter of 1976/77. In addition, a broader region of deeper mixed layers after the climate shift results in increased formation rates and mode water volumes. The surface density shift allows the outcrop of a denser layer (layer 12; $\sigma_\theta = 26.375$ kg m$^{-3}$) to move into the CMW formation region (where mixed layers are deep) resulting in increased CMW density after 1976/77. Thus, our model indicates that changes in surface density during formation are primarily responsible for CMW density variability. In contrast, Xie et al. (2000) find that, in a model forced with wind stress variability only (no heat flux variability), change in the longitudinal position of the CMW is the major mechanism for subsurface temperature variability. In other words, our simulation has CMW that essentially stays in one place but changes density, while Xie et al. (2000) show CMW that stays the same density, but moves location. This discrepancy is due to the neglect of buoyancy forcing variability in the Xie et al. model run.

To better understand the relationship between the PDO SST index (which changed sign in 1976/77) and changes in mode water formation, regressions between the PDO and various model variables were calculated. Positive PDO is associated with enhanced low pressure over the North Pacific subpolar gyre and strengthened westerly winds over a zonal band from 30° to 50°N. A positive state for the PDO is associated with deeper model mixed layers, increased formation of the denser CMW layers (layers 11 and 12), thicker layer 12 (the densest CMW layer), and an anticyclonic circulation anomaly in the densest CMW layer. Surface buoyancy forcing is the primary mechanism through which the PDO influences CMW formation. This is consistent with previous results showing that winter cooling is the primary mechanism for deepening the mixed layer in this region (Ladd and Thompson 2000).

Many studies have discussed subduction as a potential oceanic pathway from the midlatitudes to the Tropics (e.g., Deser et al. 1996; Schneider et al. 1999; Zhang and Liu 1999). Because CMW is formed in the central North Pacific where subducted temperature anomalies originate, the formation and circulation of CMW may be important in understanding the link between the midlatitudes and the Tropics. Zhang and Liu (1999) identify two preferred pathways that anomalies follow around the subtropical gyre on decadal timescales. The first pathway is the "subduction pathway" originating at the isopycnal outcrops in the northeastern part of the subtropical gyre and descending into the pycnocline on a southwestward path toward the western Tropics. The second pathway, the "subtropical pathway," originates in the eastern subtropics– Tropics and moves westward in the subtropics and then northward and eastward along the Kuroshio path toward the midlatitudes.

Anomalies introduced into the CMW at its formation region follow the subduction pathway toward the western boundary. When they reach the western boundary, they can turn toward the Tropics, possibly as coastal Kelvin waves (Lysne et al. 1997) and/or turn northward with the mean current to participate in the entrainment process that leads to the formation of new mode waters. Ladd and Thompson (2001) found that the stratification is influential in the formation of STMW and CMW. Thus, anomalous CMW formation may affect the stratification in the STMW and CMW formation regions and feed back on mode water formation decades later. This subduction/entrainment cycle is possibly another manifestation of the feedback processes proposed by Latif and Barnett (1996) and could form part of the system of feedbacks that drive decadal variability in the North Pacific. On the other hand, because the CMW, with $\sigma_\theta \sim 26.2$ kg m$^{-3}$, is deeper than the equatorial

pycnocline, even if anomalies reach the equator, they may not have any influence on tropical air–sea interaction.

In the Northern Hemisphere, exchange between the subtropics and the equator is inhibited by the high PV associated with the intertropical convergence zone (ITCZ). In contrast, no strong barrier to equatorial/subtropical exchange exists in the Southern Hemisphere. In fact, Johnson and McPhaden (1999) have shown that the exchange between the subtropical gyre and the equator in the Southern Hemisphere is much stronger than that in the Northern Hemisphere. The influence of this southern exchange may be part of the reason why Schneider et al. (1999) and others have been unable to track subducted northern anomalies all the way to the equator. Thus, the role of the Southern Hemisphere influence on the Tropics and linkages with extratropical decadal variability in both hemispheres may be important and should certainly be investigated.

Our understanding of the mechanisms responsible for decadal variability in the North Pacific has been advancing rapidly over the past decade. A variety of mechanisms and pathways may be at work in generating and maintaining decadal variability, but subduction seems to be a key factor. Because mode waters make up a large portion of the pycnocline, the role that they play in carrying anomalies from the surface to depth may be important. We have modeled only 30 years worth of variability, including an important climate shift. This period is obviously not long enough to establish the statistical significance of our results. However, these results give us a start at understanding the decadal-scale variability of CMW formation and propagation. As more data become available (longer time series, more Southern Hemisphere data), we will be able to continue to build on these results.

---

**REFERENCES**

da Silva A. M., C. C. Young, and S. Levitus, 1994: *Algorithms and Procedures*. Vol. 1, *Atlas of Surface Marine Data 1994,* NOAA Atlas NESDIS 6, 51 pp.

Deser C., M. A. Alexander, and M. S. Timlin, 1996: Upper-ocean thermal variations in the North Pacific during 1970–1991. *J. Climate*, **9**, 1840–1855. Find this article online

Deser C., 1999: Evidence for a wind-driven intensification of the Kuroshio Current Extension from the 1970s to the 1980s. *J. Climate*, **12**, 1697–1706. Find this article online

Ebbesmeyer C. C., D. R. Cayan, D. R. McClain, F. H. Nichols, D. H. Peterson, and K. T. Redmond, 1991: 1976 step in the Pacific climate: Forty environmental changes between 1968–1975 and 1977–1984. *Proc. Seventh Annual Pacific Climate Workshop (PACLIM),* Asilomar, CA, California Department of Water Resources, 115–126.

Graham N. E., 1994: Decadal-scale climate variability in the tropical and North Pacific during the 1970s and 1980s: Observations and model results. *Climate Dyn.*, **6**, 135–162. Find this article online

Hallberg R., 1995: Some aspects of the circulation in ocean basins with isopycnals intersecting sloping boundaries. Ph.D. thesis, School of Oceanography, University of Washington, 244 pp.

Hanawa K., S. Ishizaki, and Y. Tanimoto, 1996: Strengthening of wintertime midlatitude westerlies over the North Pacific since mid 1970s. *J. Meteor. Soc. Japan*, **74**, 715–721. Find this article online

Hare S. R., and R. C. Francis, 1995: Climate change and salmon production in the northeast Pacific Ocean. *Ocean Climate and Northern Fish Populations,* R. J. Beamish, Ed., Canadian Special Publication in Fisheries and Aquatic Science, 357–372.

Hautala S. L., and D. H. Roemmich, 1998: Subtropical mode water in the Northeast Pacific Basin. *J. Geophys. Res.*, **103**, 13055–13066. Find this article online

Huang R. X., and B. Qiu, 1994: Three-dimensional structure of the wind driven circulation in the subtropical North Pacific. *J. Phys. Oceanogr.*, **24**, 1608–1622. Find this article online

Inui T., K. Takeuchi, and K. Hanawa, 1999: A numerical investigation of the subduction process in response to an abrupt intensification of the westerlies. *J. Phys. Oceanogr.*, **29**, 1993–2015. Find this article online

Johnson G. C., and M. J. McPhaden, 1999: Interior pycnocline flow from the subtropical to the equatorial Pacific Ocean. *J. Phys.*

*Oceanogr.*, **29**, 3073–3089. Find this article online

Kraus E. B., and J. S. Turner, 1967: A one-dimensional model of the seasonal thermocline. II. The general theory and its consequences. *Tellus*, **19**, 98–106. Find this article online

Ladd C. A., and L. Thompson, 2000: Formation mechanisms for North Pacific central and eastern subtropical mode waters. *J. Phys. Oceanogr.*, **30**, 868–887. Find this article online

Ladd C. A., 2001: Water mass formation in an isopycnal model of the North Pacific. *J. Phys. Oceanogr.*, **31**, 1517–1537. Find this article online

Latif M., and T. P. Barnett, 1994: Causes of decadal climate variability over the North Pacific and North America. *Science*, **266**, 634–637. Find this article online

Latif M., 1996: Decadal climate variability over the North Pacific and North America: Dynamics and predictability. *J. Climate*, **9**, 2407–2423. Find this article online

Levitus S., and T. P. Boyer, 1994: *Temperature,*. Vol. 4, *World Ocean Atlas 1994,* NOAA Atlas NESDIS 4, 117 pp.

Levitus S., R. Burgett, and T. P. Boyer, 1994: *Salinity,*. Vol. 3, *World Ocean Atlas 1994,* NOAA Atlas NESDIS 3, 99 pp.

Lysne L., P. Chang, and B. Giese, 1997: Impact of the extratropical Pacific on equatorial variability. *Geophys. Res. Lett.*, **24**, 2589–2592. Find this article online

Mantua N. J., S. R. Hare, Y. Zhang, J. M. Wallace, and R. C. Francis, 1997: A Pacific interdecadal climate oscillation with impacts on salmon production. *Bull. Amer. Meteor. Soc.*, **78**, 1069–1079. Find this article online

Marshall J. C., A. J. G. Nurser, and R. G. Williams, 1993: Inferring the subduction rate and period over the North Atlantic. *J. Phys. Oceanogr.*, **23**, 1315–1329. Find this article online

Masuzawa J., 1969: Subtropical mode water. *Deep-Sea Res.*, **16**, 463–472. Find this article online

McCartney M., 1982: The subtropical recirculation of mode waters. *J. Mar. Res.*, **40**, 427–464, (Suppl.),. Find this article online

Miller A. J., D. R. Cayan, and J. M. Oberhuber, 1994: On the re-emergence of midlatitude SST anomalies. *Proc. 18th Annual Climate Diagnostic Workshop,* Boulder, CO, NOAA, 149–152.

Miller A. J., and W. White, 1998: A westward-intensified decadal change in the North Pacific thermocline and gyre-scale circulation. *J. Climate*, **11**, 3112–3127. Find this article online

Nakamura H., 1996: A pycnostad on the bottom of the ventilated portion in the central subtropical North Pacific: Its distribution and formation. *J. Oceanogr.*, **52**, 171–188. Find this article online

Namias J., 1969: Seasonal interactions between the North Pacific and the atmosphere during the 1960s. *Mon. Wea. Rev.*, **97**, 173–192. Find this article online

Namias J., 1978: Multiple causes of the North American abnormal winter of 1976–77. *Mon. Wea. Rev.*, **106**, 279–295. Find this article online

Namias J., X. Yuan, and D. R. Cayan, 1988: Persistence of North Pacific sea surface temperature and atmospheric flow patterns. *J. Climate*, **1**, 682–703. Find this article online

Nitta T., and S. Yamada, 1989: Recent warming of tropical sea surface temperature and its relationship to the Northern Hemisphere circulation. *J. Meteor. Soc. Japan*, **67**, 375–383. Find this article online

Pierce D. W., T. P. Barnett, and M. Latif, 2000: Connections between the Pacific Ocean Tropics and midlatitudes on decadal timescales. *J. Climate*, **13**, 1173–1194. Find this article online

Schneider N., A. J. Miller, M. A. Alexander, and C. Deser, 1999: Subduction of decadal North Pacific temperature anomalies: Observations and dynamics. *J. Phys. Oceanogr.*, **29**, 1056–1070. Find this article online

Suga T., Y. Takei, and K. Hanawa, 1997: Thermostad distribution in the North Pacific subtropical gyre: The central mode water and the subtropical mode water. *J. Phys. Oceanogr.*, **27**, 140–152. Find this article online

Talley L. D., 1988: Potential vorticity distribution in the North Pacific. *J. Phys. Oceanogr.*, **18**, 89–106. Find this article online

Thompson L., K. A. Kelly, D. Darr, and R. Hallberg, 2002: Buoyancy and mixed layer effects on the sea surface height response in an

isopycnal model of the North Pacific. *J. Phys. Oceanogr.,* in press.

Trenberth K. E., 1990: Recent observed interdecadal climate changes in the Northern Hemisphere. *Bull. Amer. Meteor. Soc.,* **71**, 988–993. Find this article online

Trenberth K. E., and J. W. Hurrell, 1994: Decadal atmosphere–ocean variations in the Pacific. *Climate Dyn.,* **9**, 303–319. Find this article online

Watanabe M., and T. Nitta, 1999: Decadal changes in the atmospheric circulation and associated surface climate variations in the Northern Hemisphere winter. *J. Climate,* **12**, 494–510. Find this article online

Xie S.-P., T. Kunitani, A. Kubokawa, M. Nonaka, and S. Hosoda, 2000: Interdecadal thermocline variability in the North Pacific for 1958–1997: A GCM simulation. *J. Phys. Oceanogr.,* **30**, 2798–2813. Find this article online

Yasuda T., and K. Hanawa, 1997: Decadal changes in the mode waters in the midlatitude North Pacific. *J. Phys. Oceanogr.,* **27**, 858–870. Find this article online

Zhang R.-H., and Z. Liu, 1999: Decadal thermocline variability in the North Pacific Ocean: Two pathways around the subtropical gyre. *J. Climate,* **12**, 3273–3296. Find this article online

Zhang Y., J. M. Wallace, and D. S. Battisti, 1997: ENSO-like interdecadal variability: 1900–93. *J. Climate,* **10**, 1004–1020. Find this article online

## Tables

TABLE 1. Density of model layers and the mode water masses that are found in some of the layers

| Layer index | Density ($\sigma_\theta$) | Water mass |
|---|---|---|
| 1 (Mixed layer) | Variable | |
| 2 (Buffer layer) | Variable | |
| 3 | 22.5 | |
| 4 | 23.5 | |
| 5 | 24.25 | |
| 6 | 24.75 | ESMW |
| 7 | 25.125 | STMW, ESMW |
| 8 | 25.375 | STMW, ESMW |
| 9 | 25.625 | STMW |
| 10 | 25.875 | CMW |
| 11 | 26.125 | CMW |
| 12 | 26.375 | CMW |
| 13 | 26.625 | |
| 14 | 26.875 | |
| 15 | 27.25 | |
| 16 | 27.75 | |

Click on thumbnail for full-sized image.

## Figures
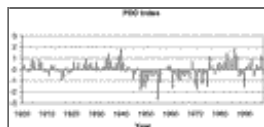


Click on thumbnail for full-sized image.

FIG. 1. Normalized winter mean (Nov–Mar) PDO index: the leading eigenvector of North Pacific SST variability [From Mantua et al. (1997).] Downloaded from the Web at ftp://ftp.atmos.washington.edu/mantua/pnw_impacts/INDICES/PDO.latest
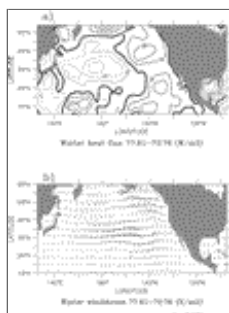


Click on thumbnail for full-sized image.

FIG. 2. Difference fields between 1977–81 and 1972–76 (a) winter heat flux (contour interval: 10 W m$^{-2}$) and (b) winter wind stress
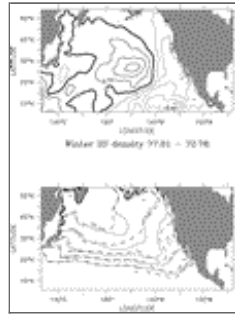


Click on thumbnail for full-sized image.

FIG. 3. (top) Winter sea surface density difference fields between 1977–81 and 1972–76 (contour interval: 0.10 kg m$^{-3}$). (bottom) Average winter surface density outcrops: 1977–81 (solid), 1972–76 (dash).
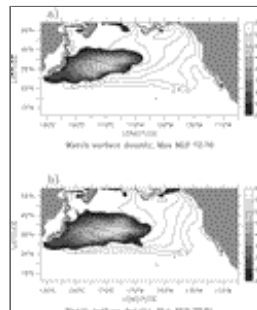


Click on thumbnail for full-sized image.

FIG. 4. Time series from the fully variable run (solid), the variable buoyancy run (dashed), and the variable wind run (dotted) for (a) CMW density, (b) STMW density, and (c) ESMW density



Click on thumbnail for full-sized image.

FIG. 5. Time series from the fully variable run (solid), the variable buoyancy run (dashed), and the variable wind run (dotted) for (a) annual maximum CMW volume and (b) annual minimum CMW volume. Means and standard deviation for 1967–76 and 1977–86 for the fully variable run are indicated



Click on thumbnail for full-sized image.

FIG. 6. March surface density (contours correspond to layer interfaces) overlaid over annual maximum mixed layer depth (shading) for the fully variable model run, averaged over (a) 1972–76 and (b) 1977–81
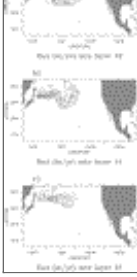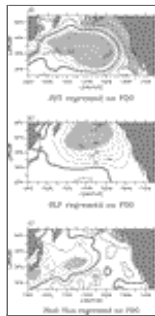
FIG. 7. Difference of annual diapycnal flux into the CMW layers between the pentads 1977–81 and 1972–76 for the fully variable model run (contour interval; 25 m yr$^{-1}$) into (a) layer 10, (b) layer 11, and (c) layer 12
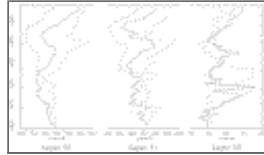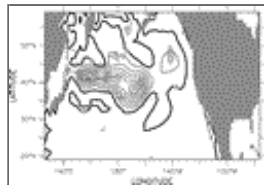
FIG. 8. Time series of the longitude of the PV minimum from the fully variable run (solid), the variable buoyancy run (dashed), and the variable wind run (dotted)
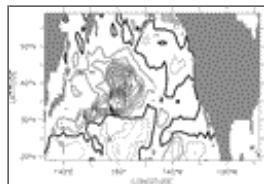
FIG. 9. Regressions on the PDO time series for (a) SST, (b) SLP, and (c) heat flux. Shading denotes regions where correlation is significantly different from zero at 95% confidence assuming a 3-yr autocorrelation timescale

FIG. 10. Regression of September thickness anomaly of the densest CMW layer (12) on the PDO time series. Shading denotes regions where correlation is significantly different from zero at 95% confidence assuming a 3-yr autocorrelation timescale

FIG. 11. Regressions of Mar mixed layer depth on the PDO time series. Shading denotes regions where correlation is significantly different from zero at 95% confidence assuming a 3-yr autocorrelation timescale

FIG. 12. Annually averaged model streamfunction in the densest CMW layer (12) regressed on the PDO time series. Shading denotes regions where correlation is significantly different from zero at 95% confidence assuming a 3-yr autocorrelation timescale

*Corresponding author address:* Carol Ladd, NOAA/PMEL, 7600 Sand Point Way, Seattle, WA 98115-6349. E-mail: cladd@pmel.noaa.gov